Supplement of Atmos. Chem. Phys., 22, 14441–14454, 2022
https://doi.org/10.5194/acp-22-14441-2022-supplement

Supplement of

Predicting atmospheric background number concentration of ice-nucleating particles in the Arctic

Guangyu Li et al.

Correspondence to: Guangyu Li (guangyu.li@env.ethz.ch), Jörg Wieder (mail@joergwieder.com), and Zamin A. Kanji (zamin.kanji@env.ethz.ch)

S1 Parameterization approach

The observed INP concentrations were obtained by two instruments, with measurements at $T = -30$ °C using HINC and from $T = -22$ to -5 °C using DRINCZ. Consider a data set with n observations and p variables (i.e., different measured temperatures). The relationship between $Y \in \mathbb{R}^{n\times p}$ (i.e., INP concentrations in logarithmic scale) and $X \in \mathbb{R}^{n\times p}$ (i.e., measured temperatures) can be fit with a linear regression with slope vector β, including the errors of the observations ϵ:

$$Y = X\beta + \epsilon, \tag{S1}$$

The linear regression with ordinary least squares (OLS) assumes constant variance in the errors (i.e., homoscedasticity). By applying OLS linear regression, however, as seen in Fig. S1 in the residual plot, heteroscedastic INP concentrations over each measured temperature are observed, which motivates the use of weighted least squares (WLS, see e.g. Strutz (2010)) linear regression to scale the median log-normal fit of INP concentrations at different temperatures. In WLS, the error term ϵ is assumed to be normally distributed with the mean value of 0 and non-uniform variance-covariance matrix E:

$$E = \begin{pmatrix} \sigma_1^2 & 0 & \cdots & 0 \\ 0 & \sigma_2^2 & \cdots & 0 \\ \vdots & \vdots & \ddots & \vdots \\ 0 & 0 & \cdots & \sigma_n^2 \end{pmatrix} \tag{S2}$$

We take the heteroscedasticity into account by dividing each observation by assigning extra non-negative weights w_i. Let the matrix W be a diagonal matrix containing these weights:

$$W = \begin{pmatrix} w_1 & 0 & \cdots & 0 \\ 0 & w_2 & \cdots & 0 \\ \vdots & \vdots & \ddots & \vdots \\ 0 & 0 & \cdots & w_n \end{pmatrix} \tag{S3}$$

The weighted least squares estimate is then:

$$\hat{\beta}_{\mathrm{WLS}} = \underset{\beta}{\arg\min} \sum_{i=1}^{n} \epsilon_i^2 = (X^T W X)^{-1}(X^T W Y), \tag{S4}$$

To minimize the effect of uneven distribution of the observed data set, the weight size in the weighing matrix W needs to be properly determined. In WLS, a typical weighing factor is to scale the standard deviation of the error ϵ_i (i.e., $w_i = 1/\sigma_i$). However, the strength and other factors depending on the intrinsic properties of the data could play a role when determining weighing sizes. As a result, to develop a linear regression within our observed INP concentrations in the exponential area and temperatures, we selected three different weighing matrices W, i.e., WLS_W$_\sigma$, WLS_W$_{\mathrm{obs}}$ and WLS_W$_{\sigma^2}$, representing weighing factor of $1/\sigma_i$, number of observations at each measured temperature, and $1/\sigma_i^2$, respectively. In Table S2, we compared the fitting parameters generated by applying different linear regression methods to the observation data set. The highest r^2 and the lowest RMSE and MAPE values were obtained for the WLS method when weighing the uneven distribution by the number of observations at each measured temperature. Therefore, the number of observations at each temperature was chosen as the weighing factor in WLS for developing the parameterization for INP concentrations. The authors suggest using the weighted least square method for future field studies when intercomparing the measurements from diverse instruments and measuring conditions to reduce the systematic bias.

S2 Time series for particle number concentration larger than $0.5\ \mu\mathrm{m}$

Figure S2 shows the aerosol number concentration for particles with physical diameter larger than $0.5\ \mu\mathrm{m}$ as function of the sample number. Each measurement lasted for three minutes for a total of 20828 and 18966 samples, from October 5–November 18, 2019, for the autumn campaign and from March 15–April 24, 2020, for the spring campaign, respectively. Observed median concentrations were 0.43 std cm^{-3} and 2.51 std cm^{-3} during the autumn and spring campaign, respectively.

S3 Overview of background and sample frozen fractions

Raw frozen fractions of all INP samples and background blanks from both seasons are presented in Figure S3. The determined background will, however, not capture accumulating contamination in the water used during sampling. INP concentrations were calculated as described in Section 2.1.1.

S4 INP concentration related to other aerosol properties

Biological particles are found to be one of the more prominent contributors to INP concentrations at warmer temperatures (T > -15°C) (Kanji et al., 2017 and references therein). During the campaign in autumn, the concentration of fluorescent particles indicative of biological particles was measured in addition to the size of the ambient aerosol. Generally, a weak correlation was observed between INP concentration and concentration of fluorescent particle concentration (see Spearman's rank coefficients per temperature in Figure S5). Given the increased correlation to the size properties in spring (see Fig. S4), it is conceivable to expect the relationship between the concentrations of INPs and fluorescent particles also to be stronger during spring.

S5 Log-normal distribution based INP parameterization

A QQ (quantile-quantile) plot provides a statistical solution to verify and visualize the hypothesized distribution (log-normal distribution in this study) of given random variables. For the variable in this study, i.e., INP concentrations at every measured temperature, the integral percentile (1 %, 2 %,..., 100 %) of the observed distribution were computed. They were consequently plotted against those from a theoretical log-normal distribution (see Fig S6). The closer the scatter points lie in a straight line, the more identical the type of distribution to the theoretical distribution for selected variables. In Figure S6, the log-normal distribution is more evident for cold nucleation temperatures, especially when $T < -12$ °C. Nevertheless, trimmed tails of the distributions can be identified at higher temperatures ($T \geq -12$ °C), where INP concentrations are biased towards the minimum detectable concentration.

Table S1. Spearman's correlation coefficients between INP concentration at different nucleation temperatures to aerosol and ambient parameters: Total aerosol concentration (n_{tot}), aerosol concentration of particles with diameter larger 0.5, 1.0, and 2.0 µm ($n_{0.5}$, $n_{1.0}$, $n_{2.0}$), aerosol surface area concentration (S), concentration of fluorescent particles (Fluorescent conc.), ambient ground temperature ($T_{\mathrm{amb.}}$), virtual ground temperature (T_{v}), potential ground temperature (θ), equivalent potential ground temperature (θ_{E}), ambient ground relative humidity ($\mathrm{RH}_{\mathrm{amb.}}$), ambient ground pressure ($p_{\mathrm{amb.}}$), ground wind direction (wd), ground wind speed (ws). Coefficients in bold represent a significant relation (significance level $p < 0.05$).

Factor	−6 °C	−8 °C	−10 °C	−12 °C	−14 °C	−16 °C	−18 °C	−20 °C	−30 °C
n_{tot} (std cm^{-3})	0.043	0.113	**0.121**	0.087	0.101	0.117	**0.161**	0.124	**0.215**
$n_{0.5}$ (std cm^{-3})	0.049	0.117	**0.126**	0.093	0.109	**0.126**	**0.167**	0.127	**0.202**
$n_{1.0}$ (std cm^{-3})	0.082	**0.154**	**0.168**	**0.138**	**0.155**	**0.167**	**0.194**	0.121	**0.213**
$n_{2.0}$ (std cm^{-3})	**0.171**	**0.265**	**0.282**	**0.259**	**0.272**	**0.276**	**0.277**	**0.173**	**0.266**
S (m^2 std cm^{-3})	0.04	**0.128**	**0.148**	**0.122**	**0.13**	**0.148**	**0.198**	**0.175**	**0.307**
Fluorescent conc. (cm^{-3})*	**0.355**	**0.311**	**0.328**	**0.321**	**0.338**	**0.273**	**0.28**	0.102	**0.22**
$T_{\mathrm{amb.}}$ (°C)	−0.021	−0.059	−0.065	−0.031	−0.05	−0.093	**−0.168**	**−0.289**	0.063
T_{v} (K)	−0.025	−0.067	−0.071	−0.047	−0.057	−0.096	**−0.179**	**−0.282**	0.063
θ (K)	−0.031	−0.057	−0.066	−0.034	−0.049	−0.091	**−0.164**	**−0.292**	0.055
θ_{E} (K)	−0.031	−0.065	−0.071	−0.042	−0.054	−0.095	**−0.172**	**−0.294**	0.053
$\mathrm{RH}_{\mathrm{amb.}}$ (%)	0.005	−0.031	−0.03	−0.057	−0.017	−0.024	−0.091	−0.096	**−0.137**
$p_{\mathrm{amb.}}$ (hPa)	**0.121**	0.061	0.091	0.105	0.061	0.062	0.007	0.042	**0.172**
wd (°)	0.044	0.014	0.016	−0.028	−0.031	0.012	−0.043	−0.005	**0.094**
ws (m/s)	**0.245**	**0.367**	**0.37**	**0.366**	**0.413**	**0.433**	**0.353**	**0.204**	**0.118**

* Note that the fluorescent particle concentration was only available for the autumn data and hence the presented correlation coefficients are restricted to autumn.

Table S2. List of parameters used for linear model fit evaluation. WLS_W_σ, WLS_W_{obs} and WLS_W_{σ^2} represent different weighing factors of the WLS linear regression model, i.e., standard deviation, number of observations at each measured temperature, and variance at each measured temperature, respectively. RMSE and MAPE symbolize the lowest root-mean-square error and mean absolute percentage error, respectively. The highlighted WLS method was selected to develop the INP parameterization in this study.

Fitting method	r^2	RMSE	MAPE (%)
OLS	0.9774	6.5708	2.2249
WLS_W_σ	0.9743	6.5791	2.3112
WLS_W_{obs}	**0.9778**	**6.5408**	**2.0302**
WLS_W_{σ^2}	0.9721	6.5899	2.4352

Table S3. List of INP measurement campaigns with associated data in the Arctic. The "Platform" column includes the ground-based (GB), ship-borne (SB) and air-borne (AB) measurements. The reported sampling technique involves filter, impactor and continuous flow diffusion chamber (CFDC); and the INP analysis method is droplet-freezing (DF), thermal diffusion chamber (TDC) and CFDC.

Reference	Observation NO.	Location	Platform	Latitude (°)	Altitude (m a.s.l)	Sampling technique	INP analysis	Sampling time	Volume (m^3 air)
[1]	2271	Ny-Ålesund, Svalbard	GB	78.9 N	11	Filter	DF	Mar 2012 - Sep 2012	213.3
[1]	5357	Alert, Canada	GB	82.5 N	210	Filter	DF	Apr 2015 - Apr 2016	16792.8
[1]	4734	Utqiagvik, Alaska	GB	71.3 N	11	Filter	DF	Jan - Aug 2013	23984.3
[1]	1323	Villum, Greenland	GB	81.6 N	24	Filter	DF	Jan - Dec 2015	5000.0
[2]	298	Ny-Ålesund, Svalbard	GB	78.9 N	475	Filter	DF	Jul 2016 and Mar 2017	15.6
[3]	96	Ny-Ålesund, Svalbard	GB	78.9 N	71	Filter	TDC	Apr 2018 and Jul 2018	9.2
[3]	622	Ny-Ålesund, Svalbard	GB	78.9 N	71	Filter	DF	Apr 2018 - Aug 2018	864.0
[4]	4	Prudhoe Bay oilfield, Alaska	GB	70.5 N	2	Impactor	DF	Mar 2017 - May 2017	38.4
[5]	3	Canadian Arctic	SB	67.2 - 81.4 N	15	Impactor	DF	Jul 2014 - Aug 2014	0.2
[6]	22	Alert, Canada	GB	82.5 N	200	Impactor	DF	Mar 2014 - Jul 2014	32.4
[7]	5	Bering sea	SB	62.6 N	20	Filter	DF	Jul 2012	13.6
[7]	3	Baffin Bay	SB	62.6 - 76.3 N	20	Filter	DF	Jul 2014	0.2
[8]	152	Arctic Ocean	SB	75.0 - 90.0 N	25	Filter	TDC	Jul 1991 - Oct 1991	3.0
[9, 20]	305	Arctic Ocean	SB	69.4 - 89.9 N	25	Filter	TDC	Jul 1996 - Sep 1996	0.6
[10]	34	Alaska	GB	71.3 N	0	Filter; CFDC	DF; CFDC	Mar 1970	3.0
[11]	27	Northern Norway	GB	69.9 N	907	Filter	DF	Jul 2015	24.0
[12]	2	Alaska, Alert and Greenland	AB	-	-	Filter	TDC	Apr 1986	1.4
[13]	15	Arctic Ocean	SB	-	-	Filter	TDC	Summer and winter 1980	1.4
[14]	38	Alert, Canada	GB	82.5 N	185	Impactor	DF	Mar 2016	1.2
[15]	2194	Villum and North Greenland Sea	AB	81.6 N	-	Filter	DF	Mar 2018 - Apr 2018	4.3
[16]	18	Villum, Greenland	GB	81.6 N	24	Filter; impinger	DF	Apr and Aug 2016	21-75; 145-800
[17]	14	Bering and Chukechi sea	SB	66.6 - 73.5 N	20	Impactor	DF	Aug - Sep 2017	39.71
[18]	1038	Ny-Ålesund, Svalbard	GB	78.9 N	474	Electrostatic precipitator	CFDC	May 2015 - Jan 2017	-
[19, 20]	12688	European Arctic Ocean	SB	66.3 - 83.7 N	-	Filter	DF	May - Jul 2017	3.3 - 13.9
[20]	825	Arctic Ocean	SB	62.5 - 90.0 N	-	Filter	DF	Jul - Aug 2001	-
[21]	10	Northern Alaska	AB	-	-	CFDC	CFDC	Jul - Oct 2004	0.06 (per hour)

[1]: Wex et al. (2019); [2]: Tobo et al. (2019); [3]: Rinaldi et al. (2021); [4]: Creamean et al. (2018); [5]: Irish et al. (2019); [6]: Mason et al. (2016); [7]: DeMott et al. (2016); [8]: Bigg (1996); [9]: Bigg and Leck (2001); [10]: Radke et al. (1976); [11]: Conen et al. (2016); [12]: Borys (1989); [13]: Borys and Grant (1983); [14]: Si et al. (2019); [15]: Hartmann et al. (2020); [16]: Šantl Temkiv et al. (2019); [17]: Creamean et al. (2019); [18]: Schrod et al. (2020); [19]: Hartmann et al. (2021); [20]: Welti et al. (2020); [21]: Prenni et al. (2009).

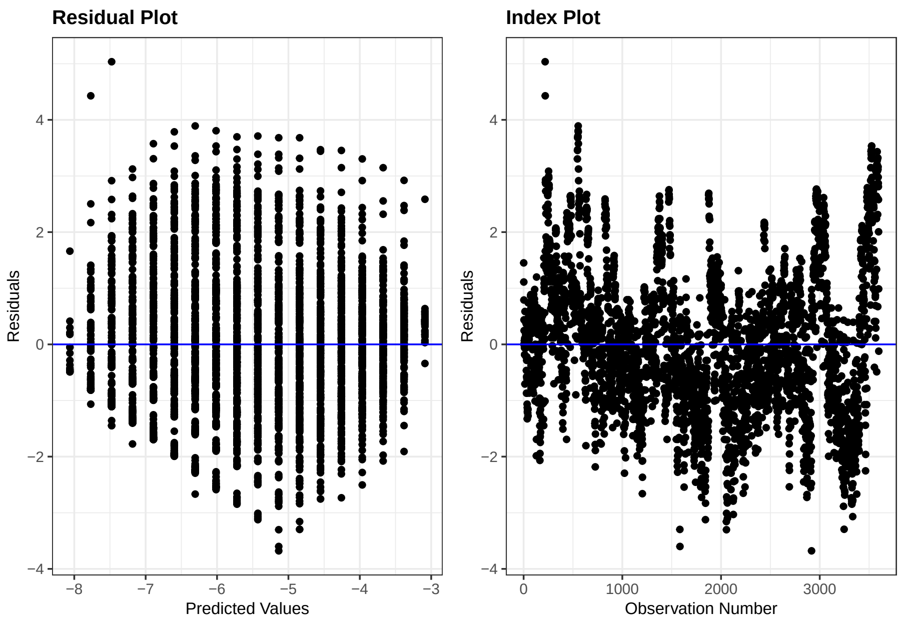

Figure S1. Left: residual distribution along the predicted values (logarithmically transformed INP concentrations). The predicted values are the power of base e. Right: residual distribution according to the index of observations.

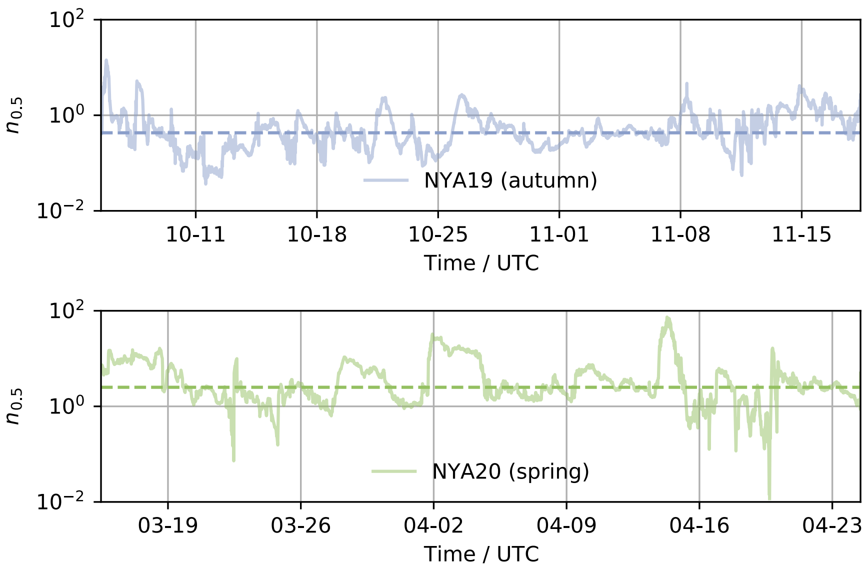

Figure S2. Time series of particle larger than $0.5\ \mu m$ physical diameter number concentration for the autumn (violet, upper panel) and spring (green, lower panel) campaign. Median concentrations for each season are indicated by the dashed horizontal lines.

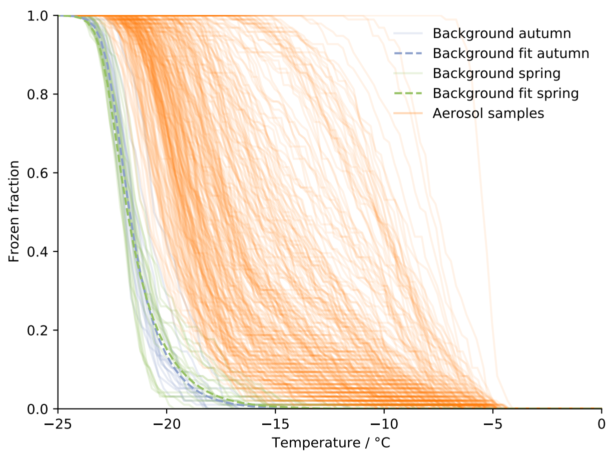

Figure S3. Overview of frozen fractions as a function of temperature obtained with DRINCZ (David et al., 2019) of background samples (blue [autumn] and green [spring]) and INP samples (orange).

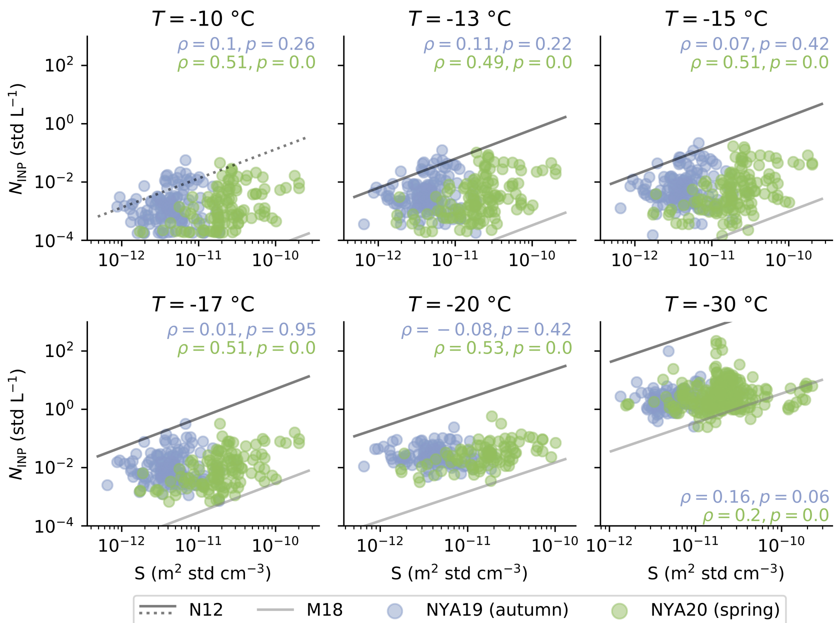

Figure S4. Observed INP concentration at selected temperatures as a function of the particle surface concentration S during sampling in the autumn (violet) and spring (green) campaign. The Spearman's rank coefficient (ρ) and p value are given for each plot. Predicted INP concentration by Niemand et al. (2012) (N12) and McCluskey et al. (2018) (M18) are presented solid black and gray, respectively. Predictions of the N12 parameterization outside of the applicable temperature range (T = -10 °C) are indicated in dashed lines.

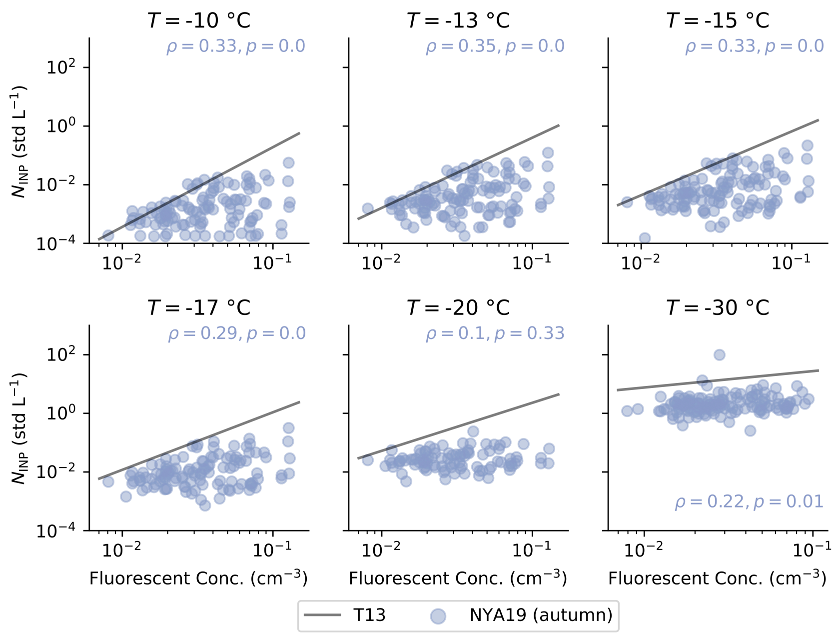

Figure S5. Observed INP concentration at selected temperatures as a function of the fluorescent particle concentration present during sampling for the autumn (violet) campaign. The Spearman's rank coefficient (ρ) and p value are given for each plot. Predicted INP concentration by Tobo et al. (2013) (T13) is presented with the solid black line.

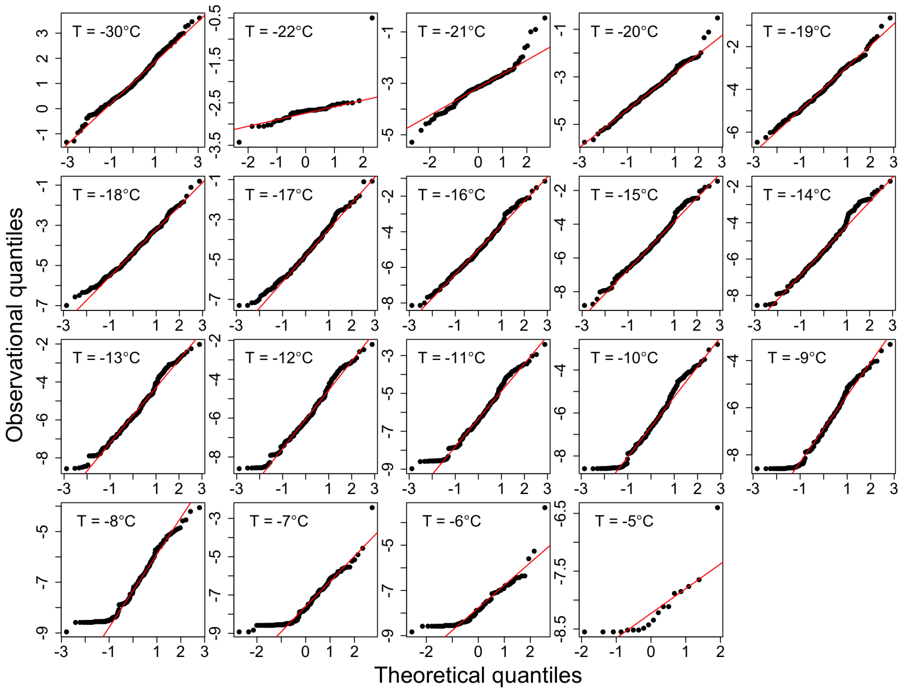

Figure S6. QQ plot (quantile-quantile plot) for INP concentrations measured at different temperatures. The value on both axes represents the exponential power to the base of e. The red solid lines are theoretical references according to the log-normal distribution.

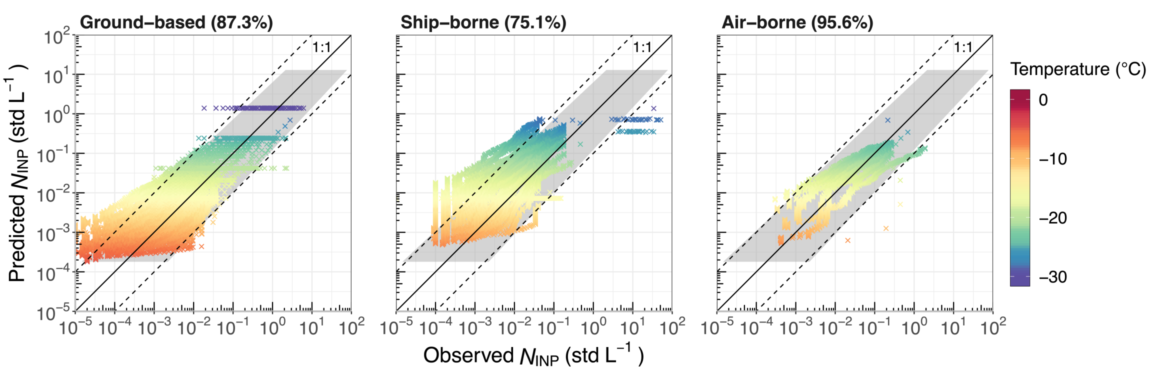

Figure S7. Predicted INP concentrations from the proposed fit (Equation 3) compared to observations from previous Arctic field campaigns per measuring platform (i.e., ground-based, ship-borne and air-borne). The values in the parenthesis represent the percentages of predicted data falling within the 95 % confidence intervals.

References

Bigg, E. K.: Ice forming nuclei in the high Arctic, Tellus B: Chemical and Physical Meteorology, 48, 223–233, https://doi.org/https://doi.org/10.3402/tellusb.v48i2.15888, 1996.

Bigg, E. K. and Leck, C.: Cloud-active particles over the central Arctic Ocean, Journal of Geophysical Research: Atmospheres, 106, 32 155–32 166, https://doi.org/https://doi.org/10.1029/1999JD901152, 2001.

Borys, R. D.: Studies of ice nucleation by Arctic aerosol on AGASP-II, Journal of Atmospheric Chemistry, 9, 169–185, https://doi.org/https://doi.org/10.1007/BF00052831, 1989.

Borys, R. D. and Grant, L. O.: Effects of long-range transport of air pollutants on Arctic cloud-active aerosol, The, Ph.D. thesis, Colorado State University. Libraries, https://doi.org/https://www.osti.gov/biblio/5100210, 1983.

Conen, F., Stopelli, E., and Zimmermann, L.: Clues that decaying leaves enrich Arctic air with ice nucleating particles, Atmospheric environment, 129, 91–94, https://doi.org/https://doi.org/10.1016/j.atmosenv.2016.01.027, 2016.

Creamean, J., Cross, J. N., Pickart, R., McRaven, L., Lin, P., Pacini, A., Hanlon, R., Schmale, D., Ceniceros, J., Aydell, T., et al.: Ice nucleating particles carried from below a phytoplankton bloom to the Arctic atmosphere, Geophysical Research Letters, 46, 8572–8581, https://doi.org/https://doi.org/10.1029/2019GL083039, 2019.

Creamean, J. M., Kirpes, R. M., Pratt, K. A., Spada, N. J., Maahn, M., Boer, G. d., Schnell, R. C., and China, S.: Marine and terrestrial influences on ice nucleating particles during continuous springtime measurements in an Arctic oilfield location, Atmospheric Chemistry and Physics, 18, 18 023–18 042, https://doi.org/https://doi.org/10.5194/acp-18-18023-2018, 2018.

David, R. O., Cascajo-Castresana, M., Brennan, K. P., Rösch, M., Els, N., Werz, J., Weichlinger, V., Boynton, L. S., Bogler, S., Borduas-Dedekind, N., Marcolli, C., and Kanji, Z. A.: Development of the DRoplet Ice Nuclei Counter Zurich (DRINCZ): Validation and application to field-collected snow samples, Atmospheric Measurement Techniques, 12, 6865–6888, https://doi.org/10.5194/amt-12-6865-2019, 2019.

DeMott, P. J., Hill, T. C., McCluskey, C. S., Prather, K. A., Collins, D. B., Sullivan, R. C., Ruppel, M. J., Mason, R. H., Irish, V. E., Lee, T., et al.: Sea spray aerosol as a unique source of ice nucleating particles, Proceedings of the National Academy of Sciences, 113, 5797–5803, https://doi.org/www.pnas.org/cgi/doi/10.1073/pnas.1514034112, 2016.

Hartmann, M., Adachi, K., Eppers, O., Haas, C., Herber, A., Holzinger, R., Hünerbein, A., Jäkel, E., Jentzsch, C., van Pinxteren, M., et al.: Wintertime airborne measurements of ice nucleating particles in the high Arctic: A hint to a marine, biogenic source for ice nucleating particles, Geophysical Research Letters, 47, e2020GL087 770, https://doi.org/https://doi.org/10.1029/2020GL087770, 2020.

Hartmann, M., Gong, X., Kecorius, S., van Pinxteren, M., Vogl, T., Welti, A., Wex, H., Zeppenfeld, S., Herrmann, H., Wiedensohler, A., et al.: Terrestrial or marine–indications towards the origin of ice-nucleating particles during melt season in the European Arctic up to 83.7° N, Atmospheric Chemistry and Physics, 21, 11 613–11 636, https://doi.org/https://doi.org/10.5194/acp-21-11613-2021, 2021.

Irish, V. E., Hanna, S. J., Willis, M. D., China, S., Thomas, J. L., Wentzell, J. J., Cirisan, A., Si, M., Leaitch, W. R., Murphy, J. G., et al.: Ice nucleating particles in the marine boundary layer in the Canadian Arctic during summer 2014, Atmospheric Chemistry and Physics, 19, 1027–1039, https://doi.org/https://doi.org/10.5194/acp-19-1027-2019, 2019.

Kanji, Z. A., Ladino, L. A., Wex, H., Boose, Y., Burkert-Kohn, M., Cziczo, D. J., and Krämer, M.: Overview of ice nucleating particles, Meteorological Monographs, 58, 1–1, https://doi.org/https://doi.org/10.1175/AMSMONOGRAPHS-D-16-0006.1, 2017.

Mason, R., Si, M., Chou, C., Irish, V., Dickie, R., Elizondo, P., Wong, R., Brintnell, M., Elsasser, M., Lassar, W., et al.: Size-resolved measurements of ice-nucleating particles at six locations in North America and one in Europe, Atmospheric Chemistry and Physics, 16, 1637–1651, https://doi.org/https://doi.org/10.5194/acp-16-1637-2016, 2016.

McCluskey, C. S., Ovadnevaite, J., Rinaldi, M., Atkinson, J., Belosi, F., Ceburnis, D., Marullo, S., Hill, T. C., Lohmann, U., Kanji, Z. A., O'Dowd, C., Kreidenweis, S. M., and DeMott, P. J.: Marine and Terrestrial Organic Ice-Nucleating Particles in Pristine Marine to Continentally Influenced Northeast Atlantic Air Masses, Journal of Geophysical Research: Atmospheres, 123, 6196–6212, https://doi.org/10.1029/2017JD028033, 2018.

Niemand, M., Möhler, O., Vogel, B., Vogel, H., Hoose, C., Connolly, P., Klein, H., Bingemer, H., Demott, P., Skrotzki, J., and Leisner, T.: A particle-surface-area-based parameterization of immersion freezing on desert dust particles, Journal of the Atmospheric Sciences, 69, 3077–3092, https://doi.org/10.1175/JAS-D-11-0249.1, 2012.

Prenni, A. J., Demott, P. J., Rogers, D. C., Kreidenweis, S. M., Mcfarquhar, G. M., Zhang, G., and Poellot, M. R.: Ice nuclei characteristics from M-PACE and their relation to ice formation in clouds, Tellus B: Chemical and Physical Meteorology, 61, 436–448, https://doi.org/https://doi.org/10.1111/j.1600-0889.2009.00415.x, 2009.

Radke, L. F., Hobbs, P. V., and Pinnons, J. E.: Observations of cloud condensation nuclei, sodium-containing particles, ice nuclei and the light-scattering coefficient near Barrow, Alaska, Journal of Applied Meteorology and Climatology, 15, 982–995, https://doi.org/https://doi.org/10.1175/1520-0450(1976)015<0982:OOCCNS>2.0.CO;2, 1976.

Rinaldi, M., Hiranuma, N., Santachiara, G., Mazzola, M., Mansour, K., Paglione, M., Rodriguez, C. A., Traversi, R., Becagli, S., Cappelletti, D., et al.: Ice-nucleating particle concentration measurements from Ny-Ålesund during the Arctic spring–summer in 2018, Atmospheric Chemistry and Physics, 21, 14 725–14 748, https://doi.org/https://doi.org/10.5194/acp-21-14725-2021, 2021.

Schrod, J., Thomson, E. S., Weber, D., Kossmann, J., Pöhlker, C., Saturno, J., Ditas, F., Artaxo, P., Clouard, V., Saurel, J.-M., et al.: Long-term deposition and condensation ice-nucleating particle measurements from four stations across the globe, Atmospheric Chemistry and Physics, 20, 15 983–16 006, https://doi.org/https://doi.org/10.5194/acp-20-15983-2020, 2020.

Si, M., Evoy, E., Yun, J., Xi, Y., Hanna, S. J., Chivulescu, A., Rawlings, K., Veber, D., Platt, A., Kunkel, D., et al.: Concentrations, composition, and sources of ice-nucleating particles in the Canadian High Arctic during spring 2016, Atmospheric Chemistry and Physics, 19, 3007–3024, https://doi.org/https://doi.org/10.5194/acp-19-3007-2019, 2019.

Strutz, T.: Data Fitting and Uncertainty (A practical introduction to weighted least squares and beyond), Springer Vieweg, 2010.

Šantl Temkiv, T., Lange, R., Beddows, D., Rauter, U., Pilgaard, S., Dall'Osto, M., Gunde-Cimerman, N., Massling, A., and Wex, H.: Biogenic sources of ice nucleating particles at the high Arctic site villum research station, Environmental science & technology, 53, 10 580–10 590, https://doi.org/https://doi.org/10.1021/acs.est.9b00991, 2019.

Tobo, Y., Prenni, A. J., DeMott, P. J., Huffman, J. A., McCluskey, C. S., Tian, G., Pöhlker, C., Pöschl, U., and Kreidenweis, S. M.: Biological aerosol particles as a key determinant of ice nuclei populations in a forest ecosystem, Journal of Geophysical Research: Atmospheres, 118, 10–100, https://doi.org/https://doi.org/10.1002/jgrd.50801, 2013.

Tobo, Y., Adachi, K., DeMott, P. J., Hill, T. C., Hamilton, D. S., Mahowald, N. M., Nagatsuka, N., Ohata, S., Uetake, J., Kondo, Y., and Koike, M.: Glacially sourced dust as a potentially significant source of ice nucleating particles, Nature Geoscience, 12, 253–258, https://doi.org/10.1038/s41561-019-0314-x, 2019.

Welti, A., Bigg, E. K., DeMott, P. J., Gong, X., Hartmann, M., Harvey, M., Henning, S., Herenz, P., Hill, T. C., Hornblow, B., et al.: Ship-based measurements of ice nuclei concentrations over the Arctic, Atlantic, Pacific and Southern oceans, Atmospheric Chemistry and Physics, 20, 15 191–15 206, https://doi.org/https://doi.org/10.5194/acp-20-15191-2020, 2020.

Wex, H., Huang, L., Zhang, W., Hung, H., Traversi, R., Becagli, S., Sheesley, R. J., Moffett, C. E., Barrett, T. E., Bossi, R., et al.: Annual variability of ice-nucleating particle concentrations at different Arctic locations, Atmospheric Chemistry and Physics, 19, 5293–5311, https://doi.org/https://doi.org/10.5194/acp-19-5293-2019, 2019.